

Extraordinarily High Minority Charge Carrier Lifetime Observed in Crystalline Silicon

Bernd Steinhauser,* Tim Niewelt,* Armin Richter, Rebekka Eberle, and Martin C. Schubert

Recent progress in surface passivation technology and wafer pretreatment already resulted in significant improvements in the achievable minority charge carrier lifetime of crystalline silicon. Herein, this is further exemplified by studying the lifetime on lowly doped crystalline silicon wafers passivated by poly-Si. To ensure credible lifetime measurements multiple measurement techniques are compared and good agreement between the investigated approaches is found. The resulting lifetime curves are analyzed in detail and the main limitation is very likely caused by silicon bulk recombination—most likely due to impurities. This analysis indicates that even very low impurity concentrations can be a limiting factor at the extraordinary high level of charge carrier lifetime observed in this study. Despite these limitations, lifetimes of 0.18 s on p-type and 0.5 s on n-type crystalline silicon wafers are measured, which to our knowledge exceed previously reported lifetimes. In both cases, these measured lifetimes correspond to an effective minority charge carrier diffusion length of ≈ 2.5 cm.

silicon wafers were achieved, both in the as-grown quality and the processing of the samples.^[1,2] Similarly, significant improvements in surface passivation^[3–6] were made allowing both higher reported effective minority charge carrier lifetimes^[5–7] as well as new record efficiencies for solar cells based on crystalline silicon.^[8–11]

This work combines the known aspects to further explore the technological limits in terms of minority charge carrier lifetimes τ_{eff} . An excellent surface passivation is applied to lowly doped high-quality crystalline silicon wafers that received the best-known pretreatment to reduce c-Si defect limitations we are aware of.^[2] The samples are characterized using multiple methods and the lifetimes acquired using these methods are compared. Furthermore, the

resulting lifetime curves are analyzed, trying to identify the nature of the observed limitations.

1. Introduction

Knowledge of the minority charge carrier lifetime in crystalline silicon (c-Si) and its limiting influences is crucial for the understanding and modeling of the performance of c-Si solar cells. In recent years, many improvements to the quality of crystalline


2. Experimental Section

To explore the practical limitations of the minority charge carrier lifetime in n- and p-type crystalline silicon, the fabricated lifetime test samples were coated with high-quality surface passivation provided by the tunnel oxide passivating contact (TOPCon)^[12] technology. Two experiments were carried out in sequence. Details on the silicon wafers is shown in Table 1. In experiment 1, the samples were first cleaned using an adapted sequence based on the cleaning sequence ($\text{HNO}_3 \rightarrow \text{HF} \rightarrow \text{SC1} \rightarrow \text{HF} \rightarrow \text{SC2} \rightarrow \text{HF}$) developed by the Radio Corporation of America followed by thermal oxidation in a tube furnace at 1050 °C to dissolve the reported float-zone (FZ) c-Si bulk defects.^[13,14] After removal of the oxide in buffered HF, the samples received a gettering step in a tube furnace at 900 °C under POCl_3 atmosphere.^[2] The phosphorus diffusion was removed in KOH followed by another cleaning with the aforementioned sequence just before surface passivation. For the surface passivation, an ultrathin oxide was grown in a tube furnace at 600 °C under N_2/O_2 atmosphere. The TOPCon layer (a-SiC_x) was deposited on both sides using a centrotherm c.PLASMA direct-plasma PECVD tool.^[5] A small amount of carbon was added to the layer to minimize the diffusion of dopants into the crystalline silicon.^[5,15] The samples were then cleaned in HNO_3 followed by HF and annealed in a tube furnace at 900 °C under N_2

B. Steinhauser, A. Richter
Advanced Development of High-Efficiency Silicon Solar Cells
Fraunhofer Institute for Solar Energy Systems
Heidenhofstr. 2, Freiburg 79110, Germany
E-mail: bernd.steinhauser@ise.fraunhofer.de

T. Niewelt, R. Eberle, M. C. Schubert
Quality Assurance, Characterization and Simulation
Fraunhofer Institute for Solar Energy Systems
Heidenhofstr. 2, Freiburg 79110, Germany
E-mail: tim.niewelt@ise.fraunhofer.de

T. Niewelt, R. Eberle
INATECH
University of Freiburg
Emmy-Noether-Straße 2, Freiburg 79110, Germany

 The ORCID identification number(s) for the author(s) of this article can be found under <https://doi.org/10.1002/solr.202100605>.

© 2021 The Authors. Solar RRL published by Wiley-VCH GmbH. This is an open access article under the terms of the Creative Commons Attribution-NonCommercial License, which permits use, distribution and reproduction in any medium, provided the original work is properly cited and is not used for commercial purposes.

DOI: 10.1002/solr.202100605

Table 1. Properties of the used FZ Si wafers. The thickness refers to the final thickness after all processing steps.

Experiment	Diameter [mm]	Sample type (Dopant)	Resistivity [Ω cm]	Final thickness [μ m]	Surface finish
1	100	n (P)	100	385	Shiny etched
1	100	p (B)	100	234	Shiny etched
2	150	n (P)	1000	480	Polished
2	150	p (B)	80	292	Polished

atmosphere. For hydrogenation, 15 nm Al_2O_3 were deposited on both sides by thermal atomic layer deposition followed by annealing in forming gas at 425 °C for 25 min.

The samples of experiment 2 were processed in the same way, except for a mechanical polishing step added between POCl_3 gettering and KOH etching.

To assess τ_{eff} , multiple techniques were used to ensure state-of-the-art high-quality measurements. First, all samples were investigated by photoconductance decay (PCD) measurements using a Sinton WCT-120 lifetime tester.^[16] The coil calibration of the used setup was carried out on a large sample set with extensive perturbation to consider the distance dependence reported by the Black et al.^[17] Both measurement modes, i.e., with a long (evaluated with the generalized method^[18]) as well as a short (evaluation of the transient) flash, were used to acquire the lifetime within different regimes of minority charge carriers densities Δn . The optical factor for the generalized evaluation was adjusted such that a good agreement with the transient decay was achieved. For the evaluation of the latter, the measurement time window was varied between 0.3 and 1.3 s to acquire more data points in mid and low Δn range, respectively.

As a second technique, photoluminescence (PL) was used using the Fraunhofer ISE modulium tool. The excitation was realized by a monochromatic continuous wave laser source with a wavelength of 790 nm. Here, two methods were applied: lifetime determination by modulated PL as well as steady-state lifetime imaging.^[19–21] For each steady-state evaluation, a background image was taken without illumination and then subtracted before calibrating the image. Neutral density (ND) filters were mounted in front of the laser optics to reduce the illumination intensity below the minimum output intensity of the used laser diode. The transmission of the ND filters was measured at the laser wavelength using a PerkinElmer Lambda 950 UV–NIR spectrometer.

To investigate possible Fe contamination, we carried out [Fe] imaging on p-type samples that were processed together with the n-type samples.^[22,23] The pairing of FeB was supported by annealing at 80 °C for 10 min in the dark before the measurement. Intense illumination was used to split them for the Fe_i measurement. The ratio of FeB to Fe_i was estimated during the calculation based on the dopant concentration and the annealing conditions.^[24]

For the modeled lifetime curve, Auger recombination was accounted for based on the upcoming model by Niewelt et al.^[25] The larger (150 mm diameter) samples were part of the sample set that was evaluated for the creation of this

Auger model. For the radiative recombination B_{low} was chosen according to Nguyen et al.,^[26] whereas B_{rel} was calculated based on the bandgap narrowing model by Schenk^[27] as suggested by Fell et al.^[28] The impact of photon recycling (PR) was assessed and accounted for according to Fell et al.^[28] Based on the equations in the referenced publication, the factor for the reabsorption of photons emitted by radiative recombination was calculated to be 96.4% for the 385 μ m thick, planar 100 Ω cm n-type sample that is mainly analyzed.

3. Comparison of Photoconductance and PL

One major goal of the investigations was to compare PL- and PCD-based methods to ensure that the measured τ_{eff} is not the result of a systematic error in the specific measurement setup. **Figure 1** shows the result of this comparison of PCD using short and long flash modes as well as modulated and steady-state PL. A good agreement of the techniques was found at $\Delta n = 4 \times 10^{15} \text{ cm}^{-3}$ or higher. For lower Δn , the modulated PL indicates lower lifetimes compared with the other techniques. The results for steady-state imaging PL instead follow the PC curves better both with and without ND filter. Measurements in the range of Δn as low as $1 \times 10^{13} \text{ cm}^{-3}$ were only achieved with PCD measurements due to the extreme lifetime level of up to 1/3 of a second. In addition, the graph also gives the radiative and Auger recombination for the chosen wafer thickness and base doping. **Figure 2** shows the calibrated τ_{eff} image for this sample at the lowest intensity possible without ND filter ($\Delta n = 4.5 \times 10^{14} \text{ cm}^{-3}$). The dashed circle indicates the approximately measurement area of the modulated PL, whereas the square indicates the area in which the lifetime was evaluated in case of steady-state imaging. The lifetime image itself indicates that the lifetime in the middle is very homogeneous at around 0.2 s. Toward the edge of the wafer, areas of lower lifetime can be observed.

While measuring τ_{eff} on typical silicon wafers (with moderate doping concentration in the range of $\approx 10^{15} - 10^{16} \text{ cm}^{-3}$) using the Sinton lifetime tester is relatively simple, in case of our wafers, there are multiple caveats, e.g., the measurement at low Δn is very sensitive to both light pollution and electronic interferences.

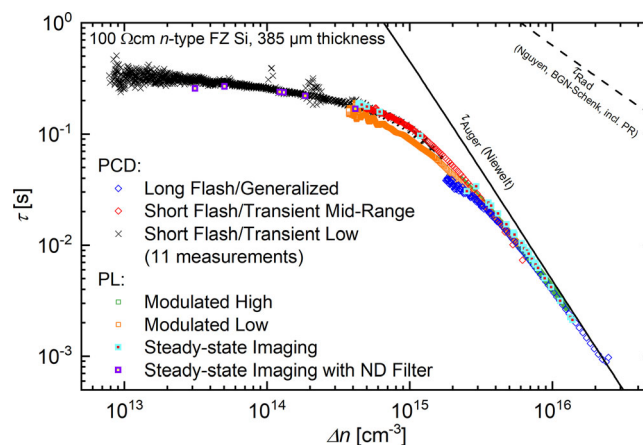


Figure 1. Measurement of the minority charge carrier lifetime on 100 Ω cm n-type FZ Si with TOPCon surface passivation. PCD and PL techniques have been compared. The solid and dashed lines indicate the Auger and radiative lifetime curves, respectively.

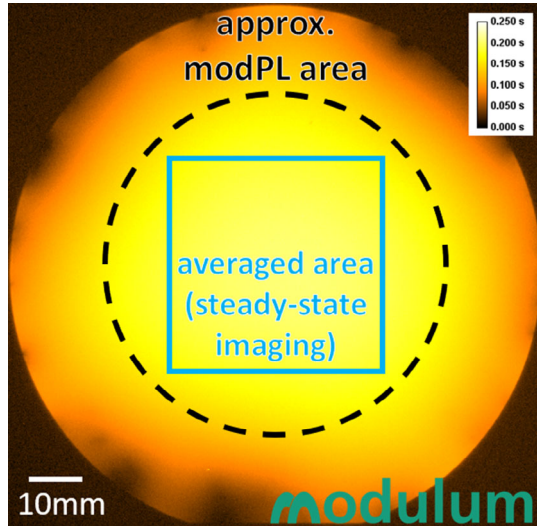


Figure 2. Lifetime-calibrated PL image on 100 Ω cm n-type FZ Si with TOPCon surface passivation at $\Delta n = 4.5 \times 10^{14} \text{ cm}^{-3}$. This corresponds to the lowest possible intensity without applying any ND filter. The calibration bar in the upper right gives the determined τ_{eff} for each color.

The observed agreement of the measured curves gives high confidence that the measured lifetime curves correspond to the actual τ_{eff} of the wafer. There is a notable deviation observed for modulated PL. This can be explained by a difference in the measured region, as shown in Figure 2. While PCD and steady-state imaging focus on a relatively small area in the middle of the wafer, the modulated PL measures a slightly larger area. Due to the defects (e.g., due to handling) present at the wafer edge and the high effective minority charge carrier diffusion length of $\approx 2.0 \text{ cm}$ at this Δn , the modulated PL is more affected by this higher recombination at the wafer edge. This influence increases with increasing diffusion length and hence with decreasing Δn . For steady-state imaging PL and PCD, the areas do not match exactly either, but the differences in the areas are much smaller. Due to this, and the good homogeneity in the center of the wafer, the results are much more comparable. This can be observed in the good agreement of the two methods over the

whole range of Δn they cover. This agreement is important as it means that the high level of the lifetime is less likely caused by measurement-specific artifacts. Especially due to the steady-state measurements dynamic artifacts like traps are much less likely to be a strong influence on the lifetime curve. Furthermore, the shape of the PCD curve around $\Delta n = 1 \times 10^{15} \text{ cm}^{-3}$ is reproduced by the steady-state imaging. In this Δn range, the radiative recombination without PR was expected to be dominant and would lead to a lower expected τ_{eff} . The shape of the measured curve can however be explained by accounting for PR. This effect, also assessed based on the data shown in Figure 1, is discussed in detail in a recent publication by Fell et al.^[28] The effect also plays a role for well-passivated c-Si featuring moderate base doping (1–5 Ω cm), where it can lead to a systematic deviation in the **surface recombination parameter** J_{0s} . This further underlines the value of these investigations, as the lifetime curve here gave direct experimental evidence of the effect of PR.

Overall, we can report the measurement of extremely high lifetimes by PCD as well as their confirmation for a large range of the measured curve with an independent second technique. This was not only important for the following analysis, but also for the analysis of more lowly doped wafers used for the new Auger model.^[25]

4. Determination of the Lifetime Limitations

With the measurement of the lifetime being established it is of course of interest whether τ_{eff} is mainly limited by surface, intrinsic bulk, or extrinsic bulk recombination, as this could lead the way to further improvement potential. To investigate the influence of the surface recombination, **Figure 3 a)** shows the measured data together with modeled lifetime curves including a variation in the J_{0s} as dashed, colored lines. Here, the J_{0s} was assumed to be injection-independent. For $J_{0s} \leq 0.5 \text{ fA cm}^{-2}$, the lifetime is strongly overestimated over almost the whole range of Δn in comparison with the measured curve. In contrast, for $J_{0s} > 2.0 \text{ fA cm}^{-2}$, the lifetime is strongly underestimated. The additional lines in the figure show the lifetime curves for radiative (dotted), Auger (dash-dotted), and total bulk recombination (solid) without surface recombination. Figure 3 b) shows the same modeled curves, but this time with an assumed additional

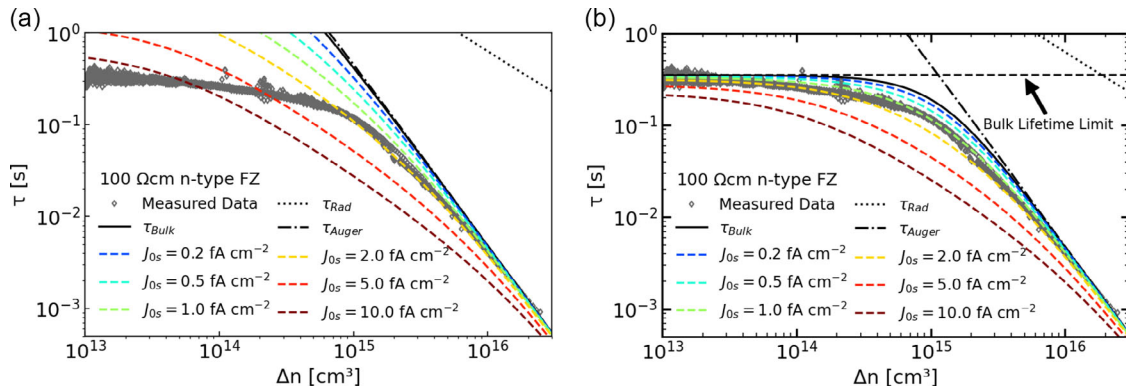


Figure 3. a) Comparison of measured and calculated minority charge carrier lifetime for varying surface recombination represented by J_{0s} . b) Similar comparison as on the left, but this time the effective lifetime is additionally limited to a constant value of 0.35 s, as indicated by the horizontal, dashed line.

constant limit of 0.35 s—indicated by the horizontal, dashed line—added to τ_{Bulk} and each curve labeled with J_{0s} . Overall, the modeled curves describe the measured curve better. Again, for $J_{0s} \leq 0.5 \text{ fA cm}^{-2}$ the lifetime is overestimated, whereas for $J_{0s} > 2.0 \text{ fA cm}^{-2}$, it is underestimated over a broad range of Δn .

This J_{0s} variation with and without the—artificial—limit indicates that only a constant, injection-independent J_{0s} cannot explain the observed τ_{eff} curve at $\Delta n < 1 \times 10^{15} \text{ cm}^{-3}$. Although the artificial limit works reasonably well, it should be supported by an actual recombination mechanism. Instead of a distribution of defects in the bandgap (as used in the classic theory of surface recombination) in this case, discrete defects are better candidates to provide an adequate injection-dependency. These are commonly described by the theory proposed by Shockley, Read, and Hall (SRH).^[29,30] If assuming, e.g., a single-level SRH bulk defect, then indeed some candidates could be found that—in 100 $\Omega \text{ cm}$ n-type c-Si—result in a (nearly) constant τ_{SRH} within the observed Δn range, e.g., Fe, V, or Mo. The required concentrations would be approximately $[\text{Fe}] = 2.8 \times 10^9$, $[\text{V}] = 8.5 \times 10^{10}$, or $[\text{Mo}] = 7.0 \times 10^8 \text{ cm}^{-3}$. Each of these defects/concentrations alone would result in a limitation of τ_{eff} to $\approx 1/3 \text{ s}$. The potential SRH defect candidates have in common that the defect energy level is below mid-bandgap and that $\sigma_n > \sigma_p$ for the capture cross sections.

In p-type c-Si, Fe imaging is a well-established method to determine the Fe concentration based on the metastable formation of FeB pairs,^[22,23] if the resulting change in the recombination rate significantly affects τ_{eff} . Due to the low required concentrations in the range from 1×10^9 to $1 \times 10^{10} \text{ cm}^{-3}$, this change in τ_{eff} due to the preparation will be low and therefore the method is very challenging and the results should be interpreted very carefully. Furthermore, this method cannot be used for n-type c-Si, as P is not known to form similar pairs with Fe. Thus, in n-type, c-Si, it is difficult to separate Fe from other defects like V or Mo. Instead, as we also processed some p-type wafers in the same batch, we applied the method to one of these wafers. Thus, if Fe was induced as an impurity during processing, it could be revealed by carrying out Fe imaging on this

sample instead. **Figure 4 a)** shows the resulting [Fe] image for a p-type 100 $\Omega \text{ cm}$ sample. In this color scale, the [Fe] concentration to match the 100 $\Omega \text{ cm}$ n-type sample would be in the red-orange range. In this color scale, most of the area—especially in the middle of the wafer—is dark, meaning that the evaluated concentration is much lower. Only very close to the wafer edge some areas indicate a significant [Fe] concentration, most likely caused by wafer handling between processes. For the area inside the yellow circle, the histogram of the concentration is shown in **Figure 4 (right)**. The panel also shows the $[\text{Fe}] = 2.8 \times 10^9 \text{ cm}^{-3}$ necessary for $\tau_{\text{SRH}} \approx 0.35 \text{ s}$ on the 100 $\Omega \text{ cm}$ n-type sample as a red dashed line. The maximum of the histogram curve is well below this dashed line. This means that the measurement would suggest a lower [Fe] concentration in the investigated p-type sample than required for a 1/3 s limitation on the n-type sample, as shown in **Figure 3**. Different concentrations on the samples could be explained by a constant dose of impurities that would be induced into the c-Si bulk during processing, as suggested by Richter et al.^[31] As the 100 $\Omega \text{ cm}$ p-type is thinner than the 100 $\Omega \text{ cm}$ n-type sample (see **Table 1**), such an approach would require the determined concentration on the 100 $\Omega \text{ cm}$ p-type used for the Fe imaging to be even higher. Hence, this approach cannot explain the discrepancy between the histogram and the dashed curve in **Figure 4 b)** either. In fact, the determined concentrations in the histogram are so low that they should not be considered to be reliable. These observations do not exclude Fe_i as a relevant impurity, but it cannot be confirmed as the main limitation this way. Nevertheless, defect recombination caused by impurities is still the most plausible candidate for the observed lifetime limitation.

One further limitation of the lifetime can be the recombination at the edge. The edge of the wafer—as shown in **Figure 2**—usually contains spots of high recombination caused by wafer handling and it is very hard to completely avoid these spots. In case of the discussed 100 $\Omega \text{ cm}$ n-type sample, the effective diffusion length L_{eff} is $\approx 2.0 \text{ cm}$ at the lowest Δn , meaning that the limitation of τ_{eff} due to the wafer edge should not yet be significant. However, if the effective lifetime is further increased

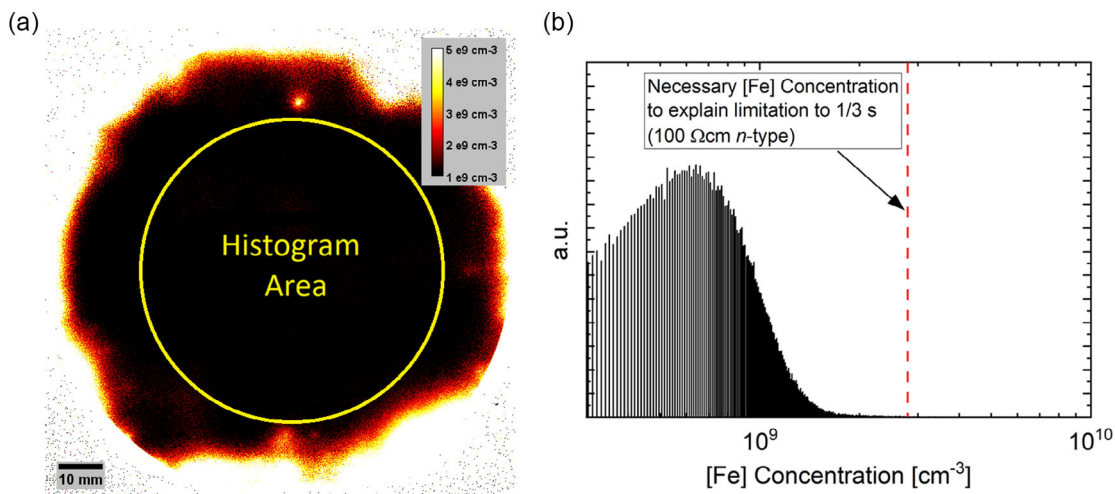


Figure 4. a) [Fe] image for the p-type 100 $\Omega \text{ cm}$ sample. b) [Fe] histogram for the shown on the left panel. The dashed red line marks the [Fe] concentration that would be necessary to limit the lifetime to 1/3 s in **Figure 3 b)** on n-type 100 $\Omega \text{ cm}$.

this will also result in an increase in L_{eff} . This can result in a limitation of τ_{eff} due to edge recombination as it was already observed for the modulated PL at lower Δn in Figure 1 due to the larger measurement area. For this reason, the practical limit on this wafer size is likely below 1 s for lowly doped n-type and even lower (around 0.2–0.3 s) on lowly doped p-type material if an unaffected area of 2–3 cm diameter should remain in the center.

5. Achieved Record Lifetimes on Crystalline Silicon

Further samples were processed based on the same fabrication processes but on larger sized wafers with 150 mm diameter. Furthermore, wafers with mechanically polished surface were used, which could lead to a minor reduction in the J_{0s} . Not all measurements shown in Section 3 and 4 could be repeated on these samples. This is the main reason why the in-depth analysis was carried out on the sample set discussed earlier.

Figure 5 shows the measured τ_{eff} curve for p-type 80 Ω cm c-Si. An effective minority charge carrier lifetime of 0.18 s was achieved on this sample. This is lower than the 1/3 s reported on the 100 mm diameter n-type sample in the previous sections. Nevertheless, L_{eff} at the maximum of the lifetime curve of this sample is ≈ 2.5 cm, which is higher than the 2.0 cm of the 100 Ω cm n-type sample discussed earlier due to the higher mobility of minority charge carriers in p-type c-Si. In addition, we used n-doped poly-Si as passivation on p-type c-Si and therefore an inversion layer forms close to the surfaces, especially on lowly doped c-Si. In accordance with the findings of Veith-Wolf et al.^[32] for Al_2O_3 layers on top of n-type wafers, we observe that for inversion, the defects at the wafer edge play a more important role compared with accumulation. Thus, the larger wafer size was a key element in achieving this high lifetime level of 0.18 s, which—to our knowledge—is the highest lifetime reported on p-type c-Si to date.

Similarly, we also applied the process to 1000 Ω cm n-type FZ Si wafers. Figure 6 shows the lifetime measured on this material indicating a minority charge carrier lifetime of up to 0.5 s. In

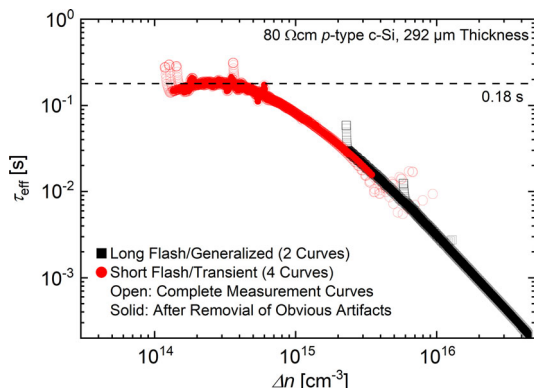


Figure 5. Minority charge carrier lifetime for 80 Ω cm p-type FZ c-Si measured by PCD. The open symbols indicate the complete measurements, whereas the solid symbols give the curves with some obvious measurement artifacts removed. The dashed line indicates a lifetime of 0.18 s.

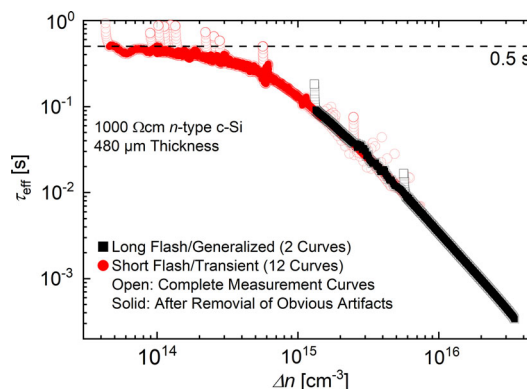


Figure 6. Minority charge carrier lifetime for 1000 Ω cm n-type c-Si measured by PCD. The open symbols indicate the complete measurements, whereas the solid symbols give the curves with some obvious measurement artifacts removed. The dashed line indicates a lifetime level of 0.5 s.

comparison with the lifetime curve shown in Figure 1, this sample could profit from the larger wafer thickness. If a certain dose of impurities was introduced during processing, as suggested by Richter et al.,^[31] the larger thickness would result in more dilution of these impurities and thus raising the limit of the lifetime correspondingly. Furthermore, the higher thickness reduces the impact of surface recombination as well. The larger wafer size of 150 mm helped to prevent hitting another possible limitation due to an increase in the diffusion length to $L_{\text{eff}} \approx 2.5$ cm. The main limitation in the lifetime at low Δn is still expected to be defect-related. Hence, a further improvement of the maximum lifetime would require investigations whether the impurity concentration in the material could be further decreased during processing. Nevertheless, 0.5 s is to our knowledge the highest lifetime that was yet observed in c-Si.

6. Conclusion

High-quality crystalline silicon wafers were thermally pretreated and subsequently passivated with TOPCon to investigate the achievable level of lifetime and investigate the limitations of the resulting lifetime curve. To ensure credible measurements, multiple measurement techniques were compared on a sample that was able to achieve a lifetime of 1/3 s finding a good agreement between the techniques. Furthermore, the data from this sample were used to model the lifetime curve to study the limitations of the lifetime. This indicated that most likely impurity-induced recombination is responsible for the limitations. Based on these findings, the process sequence was applied to another set of thicker and larger samples reaching record lifetimes of 0.18 s on p-type and 0.5 s on n-type crystalline silicon. Here the larger thickness and wafer size helped to further reduce the recombination rates.

Acknowledgements

The authors thank Dr. J. Stenzenberger and A. Lenz from Wacker AG for the kind supply of high quality FZ wafers used in this study. The authors

also thank Philipp Barth, Antonio Leimenstoll, and Felix Schätzle for processing of the samples. This work was funded by the German Federal Ministry for Economic Affairs and Energy (BMWi) under the contract numbers 0324204A and 0324204C (both LIMES). A reference was updated on November 12th, 2021.

Open access funding enabled and organized by Projekt DEAL.

Conflict of Interest

The authors declare no conflict of interest.

Data Availability Statement

Research data are not shared.

Keywords

minority charge carrier lifetime, poly-Si, silicon bulk lifetime, silicon device characterization, TOPCon

Received: August 3, 2021

Revised: August 26, 2021

Published online: September 15, 2021

- [1] N. E. Grant, V. P. Markevich, J. Mullins, A. R. Peaker, F. Rougieux, D. Macdonald, *Phys. Status Solidi RRL* **2016**, 10, 443.
- [2] T. Niewelt, A. Richter, T. C. Kho, N. E. Grant, R. S. Bonilla, B. Steinhauser, J.-I. Polzin, F. Feldmann, M. Hermle, J. D. Murphy, S. P. Phang, W. Kwapil, M. C. Schubert, *Sol. Energy Mater. Sol. Cells* **2018**, 185, 252.
- [3] F. Feldmann, M. Bivour, C. Reichel, M. Hermle, S. W. Glunz, *Sol. Energy Mater. Sol. Cells* **2014**, 120, 270.
- [4] U. Römer, R. Peibst, T. Ohrdes, B. Lim, J. Krügener, E. Bugiel, T. Wietler, R. Brendel, *Sol. Energy Mater. Sol. Cells* **2014**, 131, 85.
- [5] B. Steinhauser, J.-I. Polzin, F. Feldmann, M. Hermle, S. W. Glunz, *Sol. RRL* **2018**, 2, 1800068.
- [6] B. A. Veith-Wolf, J. Schmidt, *Phys. Status Solidi RRL* **2017**, 90, 1700235.
- [7] T. Niewelt, S. Lim, J. Holtkamp, J. Schön, W. Warta, D. Macdonald, M. C. Schubert, *Sol. Energy Mater. Sol. Cells* **2014**, 131, 117.
- [8] F. Haase, C. Hollemann, S. Schäfer, A. Merkle, M. Rienäcker, J. Krügener, R. Brendel, R. Peibst, *Sol. Energy Mater. Sol. Cells* **2018**, 186, 184.
- [9] A. Richter, R. Müller, J. Benick, F. Feldmann, B. Steinhauser, C. Reichel, A. Fell, M. Bivour, M. Hermle, S. W. Glunz, *Nat Energy* **2021**, 6, 429.
- [10] K. Yoshikawa, H. Kawasaki, W. Yoshida, T. Irie, K. Konishi, K. Nakano, T. Uto, D. Adachi, M. Kanematsu, H. Uzu, K. Yamamoto, *Nat. Energy* **2017**, 2, 17032.
- [11] D. Chen, Y. Chen, Z. Wang, J. Gong, C. Liu, Y. Zou, Y. He, Y. Wang, L. Yuan, W. Lin, R. Xia, L. Yin, X. Zhang, G. Xu, Y. Yang, H. Shen, Z. Feng, P. P. Altermatt, P. J. Verlinden, *Sol. Energy Mater. Sol. Cells* **2020**, 206, 110258.
- [12] F. Feldmann, M. Bivour, C. Reichel, M. Hermle, S. W. Glunz, *Sol. Energy Mater. Sol. Cells* **2014**, 120, 270.
- [13] N. E. Grant, V. P. Markevich, J. Mullins, A. R. Peaker, F. Rougieux, D. Macdonald, J. D. Murphy, *Phys. Status Solidi A* **2016**, 213, 2844.
- [14] A. Huber, A. Lenz, *US20190006190A1*, **2016**.
- [15] F. Feldmann, *Dissertation*, Albert-Ludwigs-Universität Freiburg, **2015**.
- [16] R. A. Sinton, A. Cuevas, *Appl. Phys. Lett.* **1996**, 69, 2510.
- [17] L. E. Black, D. H. Macdonald, *IEEE J. Photovoltaics* **2019**, 9, 1563.
- [18] H. Nagel, C. Berge, A. G. Aberle, *J. Appl. Phys.* **1999**, 86, 6218.
- [19] J. A. Giesecke, T. Niewelt, M. Rüdiger, M. Rauer, M. C. Schubert, W. Warta, *Sol. Energy Mater. Sol. Cells* **2012**, 102, 220.
- [20] J. A. Giesecke, M. C. Schubert, B. Michl, F. Schindler, W. Warta, *Sol. Energy Mater. Sol. Cells* **2011**, 95, 1011.
- [21] H. Höffler, F. Schindler, A. Brand, D. Herrmann, R. Eberle, R. Post, A. Kessel, J. Greulich, M. C. Schubert, in *37th EU PVSEC*, WIP Wirtschaft und Infrastruktur GmbH & Co Planungs KG, Lisbon **2020**, pp. 264–276.
- [22] D. Macdonald, J. Tan, T. Trupke, *J. Appl. Phys.* **2008**, 103, 73710.
- [23] M. C. Schubert, H. Habenicht, W. Warta, *IEEE J. Photovoltaics* **2011**, 1, 168.
- [24] D. Macdonald, T. Roth, P. N. K. Deenapanray, K. Bothe, P. Pohl, J. Schmidt, *J. Appl. Phys.* **2005**, 98, 83509.
- [25] T. Niewelt, B. Steinhauser, A. Richter, B. Veith-Wolf, A. Fell, B. Hammann, N. E. Grant, L. E. Black, J. Tan, A. Youssef, J. D. Murphy, J. Schmidt, M. C. Schubert, S. W. Glunz, Submitted.
- [26] H. T. Nguyen, F. E. Rougieux, B. Mitchell, D. Macdonald, *J. Appl. Phys.* **2014**, 115, 43710.
- [27] A. Schenk, *J. Appl. Phys.* **1998**, 84, 3684.
- [28] A. Fell, T. Niewelt, B. Steinhauser, F. D. Heinz, M. C. Schubert, S. W. Glunz, *Sol. Energy Mater. Sol. Cells* **2021**, 230, 111198.
- [29] W. Shockley, W. Read, *Phys. Rev.* **1952**, 87, 835.
- [30] R. Hall, *Phys. Rev.* **1952**, 87, 387.
- [31] A. Richter, J. Benick, F. Feldmann, A. Fell, M. Hermle, S. W. Glunz, *Sol. Energy Mater. Sol. Cells* **2017**, 173, 96.
- [32] B. Veith, T. Ohrdes, F. Werner, R. Brendel, P. P. Altermatt, N.-P. Harder, J. Schmidt, *Sol. Energy Mater. Sol. Cells* **2014**, 120, 436.